Sensorless Drive of Surface Mounted Permanent-Magnet Brushless DC Machines with Diametric Windings based on Inductance Measurements

Fabien Gabriel*, Frederik De Belie†, Pascal Druyts*, Xavier Neyt* and Philippe Lataire‡
*Royal Military Academy (RMA), avenue de la Renaissance 30, 1000 Brussels, Belgium
†Ghent University (UGent), St-Pietersnieuwstraat 41, 9000 Gent, Belgium
‡Vrije Universiteit Brussel (VUB), Pleinlaan 2, 1050 Elsene, Belgium

***Abstract*—Last decades, important progress have been made in sensorless control methods based on the tracking of magnetic anisotropies linked to the rotor. These methods allow to estimate the rotor position at low speed down to standstill. The magnetic anisotropy is generally approached by a sinusoidal shaped function. However, the theory must be adapted in case of additional harmonic content in the anisotropy function. This paper specifically addresses the problem for the surface-mounted permanent-magnet brushless DC machines with diametric windings. They present a peculiar magnetic anisotropy that suggests a simple method to detect the inversion of the magnetic field as a replacement to the dedicated sensors which are often used.**

***Index Terms*—AC motor drives, Brushless DC machines, Sensorless control**

I. Introduction

In sensorless control the dedicated magnetic field sensors or position sensors, required in many drives, are replaced by estimation methods using current and voltage measurements at the machine terminals only. Avoiding dedicated sensors reduces cost and improves the reliability by removing the risk of failure of these sensors [1]. Sensorless estimation methods can be classified in two main categories:

- back-electromotive force (back-emf) based methods [2]: as the back-emf is the voltage induced by the time variation of the magnetic field produced by the rotor and embraced by the stator circuits, this voltage can be used to estimate the rotor magnetic field and hence the position of the rotor. At low speed however the back-emf decreases and yields an inaccurate estimation.
- inductance-based methods [3], [4]: magnetic anisotropies may be due to the variation of the air-gap length (rotor with salient poles), or to the different local saturation levels in the iron. The anisotropies induce variations of the stator inductance and this can be used to estimated the position of the rotor. In principle these methods can be used at any speed. However, a pronounced anisotropy is required to achieve accurate estimations. Most of the permanent-magnet machines satisfy this requirement.

Many papers discuss very efficient sensorless solutions. However, most of them assume that the magnetic field density in the air gap and the magnetic anisotropy are distributed as sinusoidal functions. In permanent-magnet synchronous machines (PMSM) with trapezoidal-shaped magnetic field, often referred to as brushless DC machines (BLDCM) [5], these assumptions are not met. As a consequence, specific methods must be developed.

In [6], an initial rotor estimation method is proposed for a brushless DC motor based on the phase inductance estimation. It compares the different phase inductances with a position look-up table, but no accurate analysis is performed. In [7], the use of a look-up table correction is suggested to take into account a nonideal anisotropy in reluctance machines. In [8], measurements on a PMSM with concentrated windings are presented. The results are similar to what we have measured for BLDCM. However, the latter two do not propose explanations of the observed measurements.

This paper discusses the inductance variation as a function of the rotor position in a BLDCM with surface-mounted permanent-magnets and with diametric windings. Low load and thus small stator currents are assumed. Theoretical analysis will be compared to experimental measurements performed on a 3kW BLDCM. The inductance is estimated using injection of voltage-adaptive test-pulse sequences [9].

II. The BLDCM Model

This section describes the BLDCM with diametric windings. To highlight particularities of this type of machine, an ideal single-pole simplified model will be considered.

A. Cross-section of a BLDC

As illustrated in Fig. 1(a), the considered machine has a pair of permanent-magnets (PM) mounted on the rotor

This work is financed by the Belgian government as part of the Belgian Defense research program F0709. It is performed in collaboration with UGent in the framework of the *Interuniversity Attraction Poles* program IUAP P6/21. The UGent authors also wish to thank the *Research Foundation-Flanders* (FWO) for the financial support in the framework of project number G.0665.06.

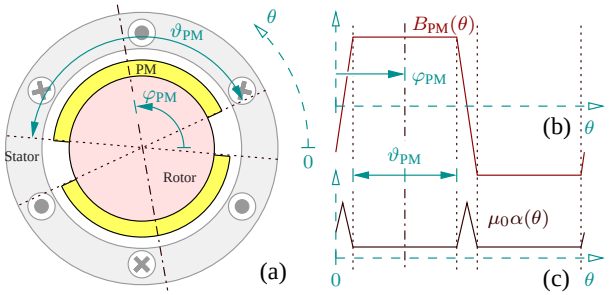

Fig. 1. Section of the BLDCM showing the rotor structure with its PM (a), PM magnetic field distribution (b), Permeability function (c)

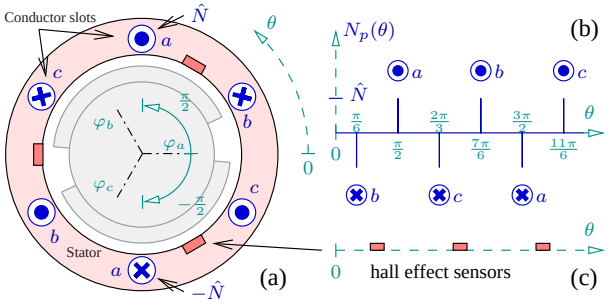

Fig. 2. Section of the BLDCM showing the stator structure with its phase conductor slots (a), Conductor distributions (b), Hall effect sensors (c)

surface. The axis of the PM forms an angle φ_{PM} with respect to the angular position $\theta = 0$. Each PM covers an angle extent ϑ_{PM}. The distribution of the magnetic field density $B_{\text{PM}}(\theta)$ produced by the PM and crossing the air-gap is constant under the PM. I.e., $B_{\text{PM}}(\theta)$ has a trapezoidal shape centered around the angle φ_{PM}, as shown in Fig. 1(b).

The considered machine has three stator phases where each phase is labeled by a letter $p \in \{a, b, c\}$. As illustrated in Fig. 2(a), a phase is made of $\hat{N}$ conductor turns wound around the phase axis defined by $\varphi_a = 0$, $\varphi_b = \frac{2\pi}{3}$ and $\varphi_c = \frac{4\pi}{3}$. The winding of a phase p is concentrated in a pair of conductor slots located at $\varphi_p + \frac{\pi}{2}$ and $\varphi_p - \frac{\pi}{2}$. Those slots contain $N_p(\varphi_p + \frac{\pi}{2}) = \hat{N}$ and $N_p(\varphi_p - \frac{\pi}{2}) = -\hat{N}$ conductors respectively and are illustrated by $\odot$ and $\otimes$ in Fig. 2. A conductor is counted positively when the current flows outside the figure for a positive current in the phase. The conductor distributions $N_p(\theta)$ are shown in Fig. 2(b), where $\odot$ and $\otimes$ are drawn to illustrate the slot locations.

The electrical current flowing in the stator phase p is noted i_p and produces, alone, a magnetic field density $B_p(\theta)$ across the air-gap. Small stator currents are assumed such that the total magnetic field density crossing the air-gap B_{total} can be approach by a linear contribution of the different magnetic sources:

$$B_{\text{total}}(\theta) = B_{\text{PM}}(\theta) + B(\theta)$$
$$\text{where} \quad B(\theta) = \sum_{p=a,b,c} B_p(\theta) \quad (1)$$

where $|B_p(\theta)| << |B_{\text{PM}}(\theta)|$. The relation between i_p and $B_p(\theta)$ is developed hereafter.

B. The anisotropic model

The magnetic anisotropy is due to the variation of the local saturation level in the iron. Small stator currents are assumed and therefore the saturation is mainly governed by the PM field. This saturation can take place in the stator and rotor yokes or in the conductor teeth [10].

Ref. [5] develops the relation between the phase currents and the magnetic induction in the air-gap from the Ampere's law $\oint_C \frac{\vec{B}}{\mu} \cdot \vec{dl} = i_{\text{enclosed}}$ in case of a machine with an infinite iron permeability, i.e. without saturation effects. If we consider a finite and variable iron permeability, that models the anisotropy, it is not possible to have such a simple expression. Therefore we propose to use a similar relation in which we have introduced a correction factor $\alpha(\theta)$ to take into account the variable saturation. It yields

$$\oint_{C(\theta_1,\theta_2)} \frac{\vec{B}}{\mu} \cdot \vec{dl} = \delta \frac{B(\theta_1)}{\mu_0 \alpha(\theta_1)} - \delta \frac{B(\theta_2)}{\mu_0 \alpha(\theta_2)} \quad (2)$$

where the closed path $C(\theta_1, \theta_2)$ crosses the air-gap at the angles θ_1 and θ_2, $\vec{B}$ is the magnetic induction, $\vec{dl}$ is the contour element vector, δ is the air-gap thickness and μ_0 is the air permeability. Assuming the design given by Fig. 1(a), the relation between $B_p(\theta)$ and i_p is

$$B_p(\theta) = H_p(\theta) \frac{\mu_0 \alpha(\theta)}{2\delta} \quad \text{where}$$
$$H_p(\theta) = \begin{cases} +i_p \hat{N} & \text{if} \quad \theta \in [\varphi_p - \frac{\pi}{2}, \varphi_p + \frac{\pi}{2}] \\ -i_p \hat{N} & \text{if} \quad \theta \in [\varphi_p + \frac{\pi}{2}, \varphi_p - \frac{\pi}{2}] \end{cases} \quad (3)$$

For diametric windings, the magnetic flux embraced by a phase p is obtained by

$$\psi_{\text{total},p} = \hat{N} \int_{\varphi_p - \frac{\pi}{2}}^{\varphi_p + \frac{\pi}{2}} B_{\text{total}}(\theta) d\theta \quad (4)$$

Using (1) in (4), the contribution of the stator currents to the magnetic flux linked by a phase p is

$$\psi_p = \hat{N} \int_{\varphi_p - \frac{\pi}{2}}^{\varphi_p + \frac{\pi}{2}} \left(\sum_{p'=a,b,c} B_{p'}(\theta) \right) d\theta \quad (5)$$

This last relation allows to compute the 3×3 inductance matrix L defined by $\Psi = LI$, where $\Psi = [\psi_a, \psi_b, \psi_c]^t$, $I = [i_a, i_b, i_c]^t$. More details are given in the appendix section VIII.

As shown in Fig. 1(c), we further assume that the permeability $\mu_0\alpha(\theta)$ is a piecewise linear function related to $B_{\text{PM}}(\theta)$. This choice of α yields good agreement with the measurements as shown in section V.

C. The traditional control

The most simple way to drive a three-phase BLDCM is to inject a current $i^\star$ and $-i^\star$ in the two phases whose conductors are in front of the PM, as shown in Fig. 3(a)(I-III). The signs of $i_p N_p(\theta)$ at the slot positions of the phase

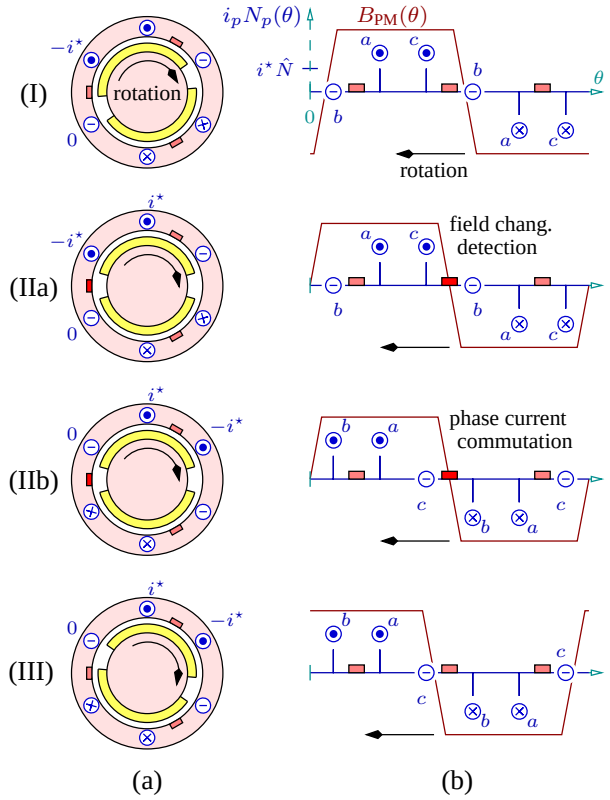

Fig. 3. For three consecutive PM orientations (I-III): Section of the BLDCM (a), superposition of the PM magnetic field, the current distributions and the hall effect sensors (b)

p are illustrated by $\odot$ and $\otimes$. No current is injected in the third phase. This is illustrated by $\ominus$.

Assuming a trapezoidal magnetic field density distribution, the torque will remain constant if the commutations occur when $\varphi_{\rm PM}$ is between $\varphi_p + k\pi + \frac{\pi-\vartheta_{\rm PM}}{2}$ and $\varphi_{p'} + k\pi + \frac{\pi+\vartheta_{\rm PM}}{2}$, where p is consecutive to p' in $\{a,b,c\}$ and k is an integer. This is illustrated in Fig. 3: at the positions (IIa), a hall effect sensor detects an inversion of the field in the air-gap and initiates a commutation between the phases c and b, as shown in (IIb).

This control technique requires the detection of the orientation of the PM-rotor. For this, hall effect sensors are usually used in the control loop. The goal of the sensorless BLDCM-control is to estimate the PM-rotor position without any dedicated sensor, such as hall effect sensors. A solution based on the inductance variation is proposed hereafter. In this paper a continuous variation of the currents i_p is considered.

III. The Inductances

This section analyzes the inductances obtained from the simple model described in the previous section. The space vector formalism, also called space phasor, is used for the electromagnetic variables. This is indicated by using underlined letters. The space vectors in a reference-frame related to the stator result from the Clarke transformation applied to the phase variables [11], [12]: $\underline{x} = C'X$, where $X = [x_a, x_b, x_c]^t$ contains the phase variables and C' is the transformation matrix. This yields convenient two-dimensional vectors that can be superimposed on the machine section. Assuming $x_a + x_b + x_c = 0$, we also have $X = C\underline{x}$, where $I^{(2\times2)} = CC'$.

In any $\alpha\beta$ reference-frame rotated by an angle $\varphi_{\alpha\beta}$ with respect to the stator reference-frame, the coordinates of the space vector $\underline{x}_{\alpha\beta} = [x_\alpha, x_\beta]^t$ are given by:

$$\underline{x}_{\alpha\beta} = \underbrace{\begin{bmatrix} \cos\varphi_{\alpha\beta} & \sin\varphi_{\alpha\beta} \\ -\sin\varphi_{\alpha\beta} & \cos\varphi_{\alpha\beta} \end{bmatrix} \underline{x}}_{\underline{x}^{\angle-\varphi_{\alpha\beta}}} \tag{6}$$

where $\angle$ indicates the rotation operation. Without index, $\underline{x}$ is defined in the stator reference-frame.

A. Flux produced by the stator currents

In a reference-frame related to the stator, let's define the space vector of the stator currents $\underline{i}$ and its orientation φ_i. The space vector of the flux $\underline{\psi}$ induced by the contribution of the stator currents is related to $\underline{i}$ by $\underline{\psi} = \boldsymbol{l}\underline{i}$, where

$$\boldsymbol{l} = C'LC \tag{7}$$

is a 2×2 inductance matrix. Note that the space vector of embraced fluxes, such as $\underline{\psi}$, is a mathematical object that does not define the entire magnetic field distribution since this distribution is not a sinusoidal function.

B. Inductances assuming a fixed rotor

The permeability function $\mu_0\alpha(\theta)$ is fixed if the PM-rotor is fixed. As a result, the inductance matrix L computed using (5) and the inductance $\boldsymbol{l}$ computed using (7) are constant. As L, and therefore $\boldsymbol{l}$, are symmetrical, it is always possible to find a reference-frame, noted xy, oriented such that $\boldsymbol{l}$ is a diagonal matrix:

$$\underline{\psi}_{xy} = \begin{pmatrix} l_x & 0 \\ 0 & l_y \end{pmatrix} \underline{i}_{xy} \tag{8}$$

This relation can also be written

$$\underline{\psi}_{xy} = l_C\underline{i}_{xy} + l_\Delta\underline{i}^*_{xy} \tag{9}$$

where $\underline{i}^*_{xy} = [i_x, -i_y]^t$ and where the inductance factors are [7]:

$$l_C = \frac{l_x + l_y}{2} \quad \text{and} \quad l_\Delta = \frac{l_x - l_y}{2} \tag{10}$$

Since the space vector $\underline{i}^*_{xy}$ is rotating in a reverse direction, using (6), we have :

$$\underline{i}^*_{xy} = \left(\underline{i}^{\angle-\varphi_{xy}}\right)^* = \underline{i}^{*\angle\varphi_{xy}} \tag{11}$$

where φ_{xy} is the angle of the xy reference-frame with respect to the stator reference-frame. Using (6) and (11), (9) yields in the stator reference-frame:

$$\underline{\psi} = l_C\underline{i} + l_\Delta\underline{i}^{*\angle2\varphi_{xy}} \tag{12}$$

We define $\underline{\psi}_C$ as the part of the flux that rotates with $\underline{i}$, and $\underline{\psi}_\Delta$ as the part that rotates reversely with $\underline{i}$:

$$\begin{aligned} \underline{\psi}_C &= l_C\underline{i} \\ \underline{\psi}_\Delta &= l_\Delta\underline{i}^{*\angle2\varphi_{xy}} \end{aligned} \tag{13}$$

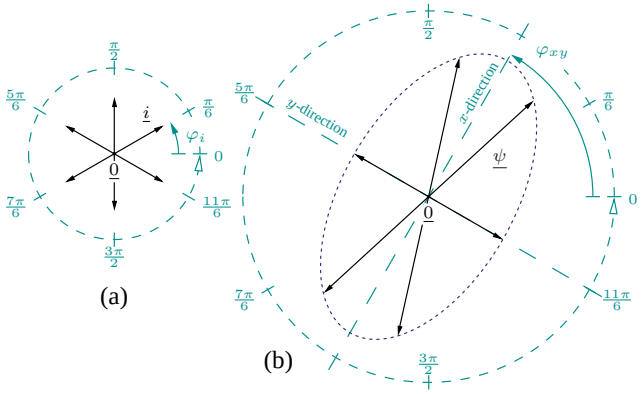

Fig. 4. Space vector of the flux $\underline{\psi}$ (b) drawing an ellipse, shown by a blue dashed line, when φ_i continuously variates. The locus of $\underline{\psi}$ is represented for different typical orientations $\underline{i}$ (a), with $\varphi_{\mathrm{PM}} = \frac{5\pi}{6}$.

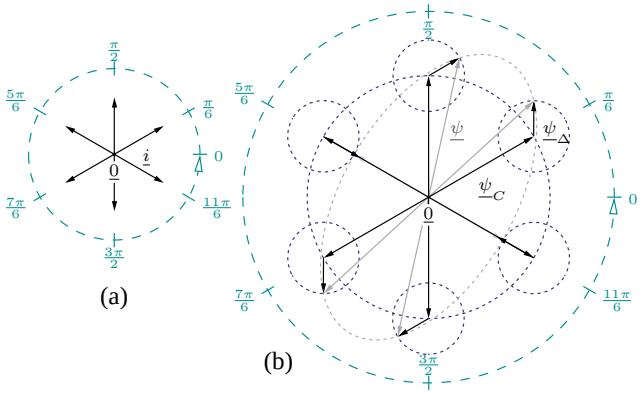

Fig. 5. Decomposition of the space vector of the magnetic flux $\underline{\psi}$ (b) in two rotating vectors $\underline{\psi}_C$ and $\underline{\psi}_\Delta$, shown by blue dashed lines. The locus are represented for different typical orientations $\underline{i}$ (a), with $\varphi_{\mathrm{PM}} = \frac{5\pi}{6}$.

Fig. 4 illustrates the elliptic variation of $\underline{\psi}$ when $\underline{i}$ rotates. The x and y directions of the xy reference-frame are depicted by turquoise dashed straight lines. Some typical orientations of $\underline{i}$ are shown. They corresponds to the values that take the phase currents in the traditional control, as explained in section II-C. Fig. 5 illustrates the decomposition of $\underline{\psi}$ in the two rotating parts $\underline{\psi}_C$ and $\underline{\psi}_\Delta$.

The xy-orientation is related to the PM-rotor position, but is not necessarily oriented along the PM-axis in case of additional harmonic content in the permeability function. The effect of the PM-orientation on the xy-orientation and on the inductance factors is analyzed hereafter.

C. Effect of the PM rotation

During the rotation of the PM-rotor, the different circuits links a moving permeability $\mu_0\alpha(\theta)$. For seven different angles between $\pi/2$ and $\pi/6$ and assuming a constant space vector of the currents orientated by $\varphi_i = \pi/6$, Fig. 6(c-e) shows the contribution of the circuits a, b and c to the magnetic field distribution calculated using (3) and assuming the permeability function given by Fig. 6(b). Fig. 6(f) shows the corresponding space vector of the flux

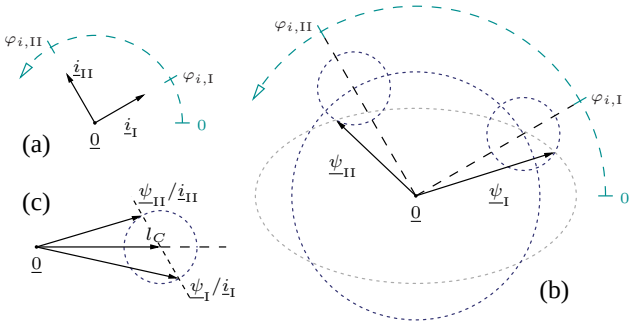

Fig. 7. The space vectors $\underline{\psi}_{\mathrm{I}}$ and $\underline{\psi}_{\mathrm{II}}$ (b) respectively for two space vectors $\underline{i}_{\mathrm{I}}$ and $\underline{i}_{\mathrm{II}}$ oriented in quadrature (a), and a graphical construction of $l_C = |(\underline{\psi}_{\mathrm{I}}/\underline{i}_{\mathrm{I}} + \underline{\psi}_{\mathrm{II}}/\underline{i}_{\mathrm{II}})/2|$, with $\varphi_{\mathrm{PM}} = \frac{\pi}{2}$.

$\underline{\psi}$. The blue dashed triangle in Fig. 6(f) illustrates the locus of $\underline{\psi}$ during the whole rotation. The explanation is given hereafter.

The flux ψ_p given by (5) is the sum of the surface under the curves Fig. 6(c-e) between the two conductor slot positions of the phase p, multiplied by $\hat{N}$. Between Fig. 6(I)-(II) and between (VI)-(V), there is no variation of the different ψ_p while the PM are in front of the conductors. The space vector $\underline{\psi}$ is therefore constant. Between (II)-(VI) however, the magnetic field distributions vary. It can be shown that the space vector $\underline{\psi}$ varies along a straight line. More details are given in the appendix section VIII.

As described in section III-B, $\underline{\psi}$ can be decomposed in $\underline{\psi}_C$ and $\underline{\psi}_\Delta$ at any PM-rotor angle, as shown in Fig. 6(f). We can deduce that $\underline{\psi}_C$ remains the constant at any PM-rotor angle and is at the center of the triangle. Therefore l_C remains also constant at any PM-rotor angle. We see hereafter how to analyze the effect of the variation of the PM-rotor angle on $\underline{\psi}_\Delta$. Note that the triangle rotates reversely with $\underline{i}$ since it corresponds to the locus of $\underline{\psi}_\Delta$.

D. The space vector inductance

For convenience, we define a space vector inductance $\underline{l}_\Delta$ by:

$$\underline{l}_\Delta = \underline{\psi}_\Delta / \underline{i}^* \tag{14}$$

Note that many authors such as [13] define the space vector inductance dividing by $\underline{i}$ instead of $\underline{i}^*$. The advantage of our definition is that $\underline{l}_\Delta$ is independent of $\underline{i}$. Using (13), (14) yields

$$\underline{l}_\Delta = l_\Delta \underline{1}_0^{\angle 2\varphi_{xy}} \tag{15}$$

where $\underline{1}_0 = [1, 0]^t$. Therefore, we have $|\underline{l}_\Delta| = l_\Delta$ and $\mathrm{angle}(\underline{l}_\Delta) = 2\varphi_{xy}$.

E. Estimation of the inductances

In practice, $\underline{\psi}$ is generally estimated from signal-injection-based techniques [9]. Our first objective is to estimate the part $\underline{\psi}_\Delta$ in order to compute (14). For this, it is important to compute $\underline{\psi}_C$ from a good estimation of l_C. This estimation can be performed from two measurements of $\underline{\psi}$ in two different orientations φ_i, e.g. in quadrature

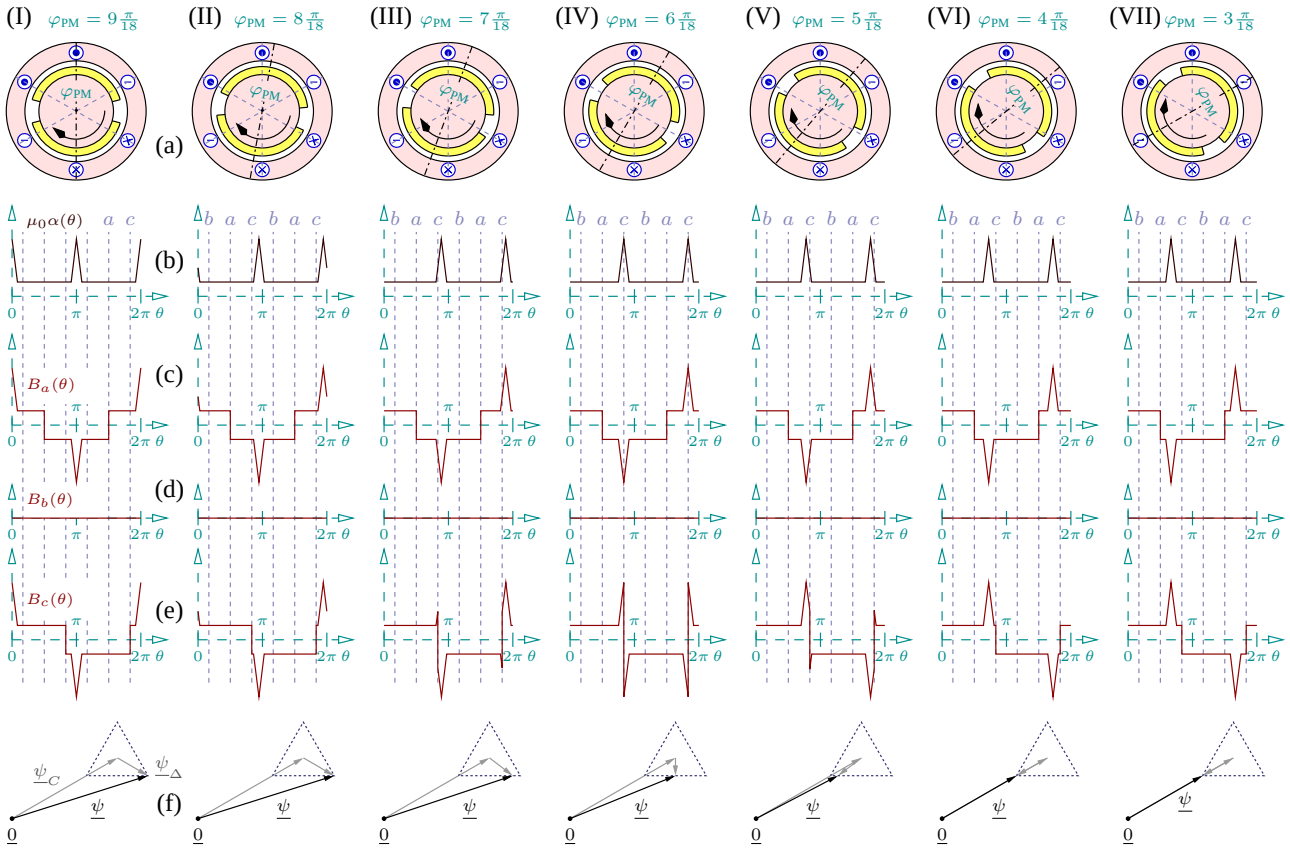

Fig. 6. For seven consecutive PM-rotor orientations between $\pi/2$ and $\pi/6$ (I-VII) and assuming $\varphi_i = \pi/6$: section of the BLDCM (a), permeability function (b), contribution of the phases a, b and c to the magnetic field density (c-e) and space vector of the fluxes linked to the contribution of the phase currents (d). The blue dashed triangle represents the locus of the space vector as a function of $\varphi_{\rm PM}$.

as illustrated in Fig. 7. These measurements should be performed in a short period of time compared to the rotation speed of the machine, in order to have only small variations of $\varphi_{\rm PM}$. Then $\underline{l}_\Delta$ is computed from $\underline{\psi}_\Delta = \underline{\psi} - l_C\underline{i}$ using (14).

IV. Simulation Results

A. Simulation data

The simulation is based on a PM-rotor angle extent of $\vartheta_{\rm PM} = 0.85\pi$. The exact amplitude of $\alpha(\theta)$ is not specified as it only influences the size of the triangle, but not the shape.

B. Results

Fig. 8(a) illustrates the locus of $\underline{l}_\Delta$, indicating some specific $\varphi_{\rm PM}$ positions. Fig. 9(a) and Fig. 10(a) show respectively the inductance l_Δ and the xy-orientation φ_{xy} as a function of $\varphi_{\rm PM} + \frac{\pi}{2}$. We choose $\varphi_{\rm PM} + \frac{\pi}{2}$ as it corresponds to the maximum of the anisotropic permeability $\mu(\theta)$ illustrated in Fig. 1.

We observe that the relation between φ_{xy} and $\varphi_{\rm PM}$ is strongly nonlinear. As a result, it will be difficult to accurately derive the orientation of the PM-rotor from φ_{xy}. It is however possible to use it to track the transition from one PM-rotor pole to the other. Note that φ_{xy} is a π-periodical value. This introduces an well-known initial uncertainty in the estimation of $\varphi_{\rm PM}$ that must be initially removed [14], [15].

The inductance l_Δ can also be used to track the transition from one PM-rotor pole to the other if its variations are pronounced.

V. Experimental Results

A. Experimental set-up

The experimental BLDCM is a 3kW in-wheel motor developed by *Technicréa*, France, for the propulsion of small vehicles. Information about the design can be found in [16]. Its stator inductance varies around l_C =90μH and the resistor is about 0.2Ω, including the 1.4 meters power cables connecting the machine to the voltage-source. Its nominal electrical rotation frequency is about 120Hz. With 14 pole-pairs, this corresponds to a nominal mechanical rotation speed of about 500rpm. The machine is fed with an IGBT voltage-source inverter from *SEMIKRON* connected to a DC voltage rectifier. Low DC-voltage of about 50V is used to limit the amplitude of the currents ripples. The PWM generator works at 10kHz. Using such a low DC voltage and high switching periods reveals important nonlinearities in the inverter, such as the voltage drop across the semiconductors or the *zero-clamp phenomenon*.

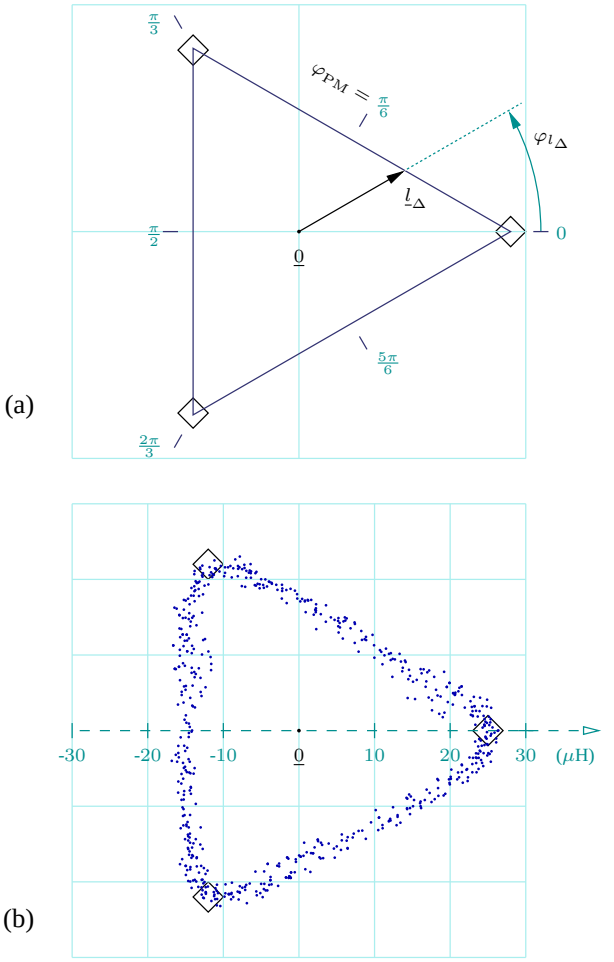

Fig. 8. Simulated locus (a) and experimental locus (b) of $\underline{l}_\Delta$ when φ_{PM} varies.

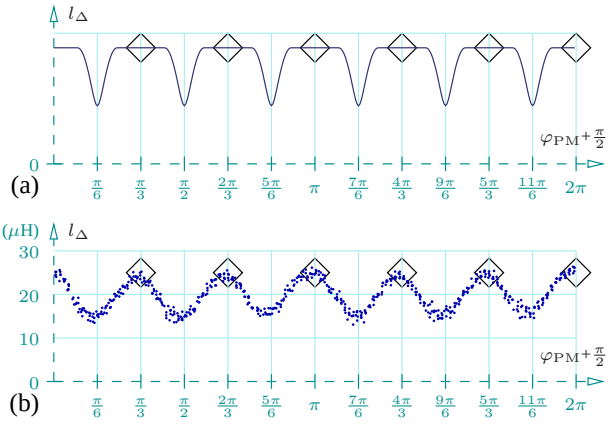

Fig. 9. Simulated value (a) and experimental value (b) of l_Δ as a function of $\varphi_{\mathrm{PM}} + \frac{\pi}{2}$.

Those nonlinearities are taken into account as discussed in [17], [18].

B. Estimation method

To estimate the inductance, test-pulses are injected every 8 switching periods, i.e., every 0.8ms, in addition to the normal operating voltage. The resulting high frequency current response is extracted from the current sensor measurements and used to calculate the inductance. Note that the test-pulses are made *adaptive* [9] and take into account the additional resistive voltage drop in order to reduce their impact on the current controller of the machine driver [17].

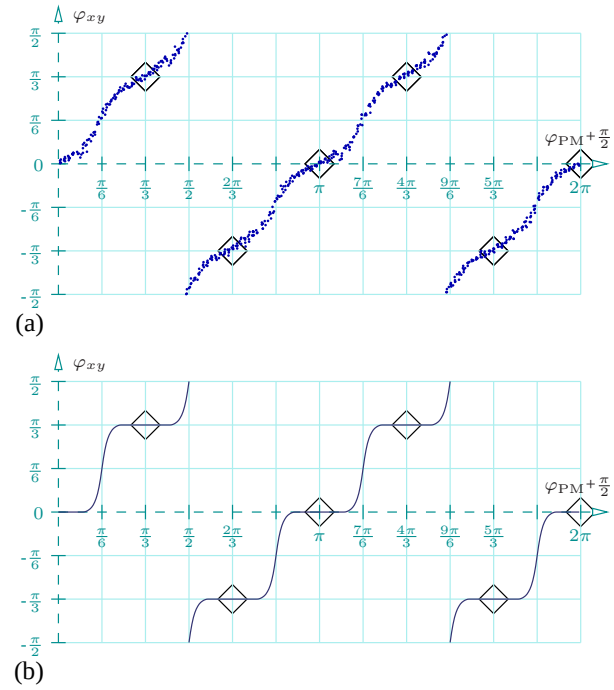

Fig. 10. Simulated value (a) and experimental value (b) of φ_{xy} as a function of $\varphi_{\mathrm{PM}} + \frac{\pi}{2}$.

C. Measurements

The measurements are taken with the machine unloaded, to have small stator currents, and rotating at an electrical frequency of 10Hz, about 10% of the rated speed. In order to keep the rotation speed as constant as possible, an encoder feedback is used in the controller. Results, assuming a correct knowledge of l_C, are shown in Fig. 8(b), Fig. 9(b) and Fig. 10(b). One can see that the experimental results are in good agreement with the results predicted by our model. However the measurements show rounded corners on the triangle which might be related to the fact that the permeability function is not exactly constant under the PM. These results are very satisfactory for use in sensorless control.

Note that such triangular locus have already be observed in previous experiments such as [8].

VI. Sensorless Control

Instead of using the dedicated sensors to control the phase commutation, it is suggested to use a inductance-based sensorless control method where the position of the phase commutations are estimated from the computation of (14). To satisfying the conditions for a constant torque, the commutations should occur between two corners of the triangles shown by diamonds in Fig. 8, Fig. 9 and Fig. 10.

VII. Conclusion

In this paper, a model for the variation of the inductance as a function of the PM-rotor position is discussed for a surface-mounted PM Brushless DC machine with diametric windings. The model can be used to detect the rotor position in a sensorless way by injecting high-frequency test-pulses signals. The model is verified by comparing simulation results with experimental data. Further research will focus on the effect of larger stator currents that will typically exist when the machine is loaded.

VIII. Appendix

Replacing $B_{p'}(\theta)$ by (3), (5) yields

$$\psi_p = \hat{N}^2 \frac{\mu_0}{2\delta} \left((i_p - i_q + i_r) \int_{\varphi_p - \frac{\pi}{2}}^{\varphi_p - \frac{\pi}{6}} \alpha(\theta) d\theta + (i_p - i_q - i_r) \int_{\varphi_p - \frac{\pi}{6}}^{\varphi_p + \frac{\pi}{6}} \alpha(\theta) d\theta + (i_p + i_q - i_r) \int_{\varphi_p + \frac{\pi}{6}}^{\varphi_p + \frac{\pi}{2}} \alpha(\theta) d\theta \right) \quad (16)$$

where q is consecutive to p and r is consecutive to q in $\{a, b, c\}$. Let's define $\mathcal{A}_p$ as the following integral

$$\mathcal{A}_p = \int_{\varphi_p - \frac{\pi}{6}}^{\varphi_p + \frac{\pi}{6}} \alpha(\theta) d\theta \quad (17)$$

If we assume that $\alpha(\theta)$ is symmetrical in φ_{PM}, we have

$$\mathcal{A}_q = \int_{\varphi_p - \frac{\pi}{2}}^{\varphi_p - \frac{\pi}{6}} \alpha(\theta) d\theta \quad \text{and} \quad \mathcal{A}_r = \int_{\varphi_p + \frac{\pi}{6}}^{\varphi_p + \frac{\pi}{2}} \alpha(\theta) d\theta \quad (18)$$

Therefore, (16) yields

$$\psi_p = \hat{N}^2 \frac{\mu_0}{2\delta} \left(i_p \left(\mathcal{A}_p + \mathcal{A}_q + \mathcal{A}_r \right) + i_q \left(\mathcal{A}_r - \mathcal{A}_p - \mathcal{A}_q \right) + i_r \left(\mathcal{A}_q - \mathcal{A}_p - \mathcal{A}_r \right) \right) \quad (19)$$

From (19), we can extract the matrix of the phase inductances L. Applying (7) on L yields:

$$\boldsymbol{l} = \hat{N}^2 \frac{\mu_0}{2\delta} \begin{bmatrix} \frac{2}{3}\left(4\mathcal{A}_a + \mathcal{A}_b + \mathcal{A}_c\right) & \frac{2}{\sqrt{3}}\left(\mathcal{A}_c - \mathcal{A}_b\right) \\ \frac{2}{\sqrt{3}}\left(\mathcal{A}_c - \mathcal{A}_b\right) & 2\left(\mathcal{A}_b + \mathcal{A}_c\right) \end{bmatrix} \quad (20)$$

Note that $\mathcal{A}_a$, $\mathcal{A}_b$, $\mathcal{A}_c$ are functions of φ_{PM} and that $\mathcal{A}_a + \mathcal{A}_b + \mathcal{A}_c$ is constant:

$$\mathcal{A}_a + \mathcal{A}_b + \mathcal{A}_c = \frac{1}{2} \oint \alpha(\theta) d\theta = \mathrm{const} \quad (21)$$

Assume the function $\alpha(\theta)$ given in Fig. 6(b). During the transition of one PM-pole to the other in front of the slots of the phase p, remark that $\mathcal{A}_p$ remains constant. Therefore the expression (20) can be simplified using only one variable $\mathcal{A}'$ that is a combination of $\mathcal{A}_a$, $\mathcal{A}_b$ and $\mathcal{A}_c$. By consequence, $\underline{\psi}$ varies along a straight line.

References

[1] T.-H. Kim, H.-W. Lee, and M. Ehsani, "State of the art and future trends in position sensorless brushless dc motor/generator drives," in *Industrial Electronics Society Conference (IECON)*, pp. 1718 – 1725, Nov. 2005.

[2] J. Johnson, M. Ehsani, and Y. Guzelgunler, "Review of sensorless methods for brushless dc," in *IEEE Industry Applications Conference (IAS)*, vol. 1, 1999.

[3] M. Schroedl, "Detection of the rotor position of a permanent magnet synchronous machine at standstill," *Proc. ICEM, Pisa, Italy*, pp. 195 – 197, 1988.

[4] A. Consoli, G. Scarcella, and A. Testa, "Sensorless control of ac motors at zero speed," in *Proceedings of the IEEE ISIE*, vol. 1, pp. 373 – 379, 1999.

[5] J. Chiasson, *Modeling and high performance control of electric machines*. USA: IEEE Computer Society Press, 2005.

[6] S. Shan, L. Qingfu, X. Wei, and W. Xinghua, "A novel starting method for the sensorless salient-pole brushless dc motors," in *Conference on Electrical Machines and Systems (ICEMS)*, vol. 2, pp. 895 – 897, Aug. 2001.

[7] P. Landsmann, R. Kennel, H. de Kock, and M. Kamper, "Fundamental saliency based encoderless control for reluctance synchronous machines," in *International Conference on Electrical Machines (ICEM)*, Sept. 2010.

[8] F. Demmelmayr, A. Eilenberger, and M. Schroedl, "Sensorless electric traction drive with 500 Nm outer rotor permanent magnet synchronous machine," in *International Conference on Electrical Machines (ICEM)*, Sept. 2010.

[9] F. De Belie, P. Sergeant, and J. Melkebeek, "A sensorless drive by applying test pulses without affecting the average-current samples," *IEEE Transactions on Power Electronics*, vol. 25, no. 4, pp. 875 – 888, 2010.

[10] J. Moreira and T. Lipo, "Modeling of saturated ac machines including air gap flux harmonic components," *IEEE Transactions on Industry Applications*, vol. 28, pp. 343 – 349, Mar/Apr 1992.

[11] R. H. Park, "Two-reaction theory of synchronous machines: Generalized method of analysis - part i," *American Institute of Electrical Engineers (AIEE)*, pp. 716 – 727, July 1929.

[12] P. Vas, *Electrical Machines and Drives: A Space-Vector Theory Approach*. United States: Oxford University Press, 1993. From inter-universitary loan.

[13] F. D. Belie, J. Melkebeek, K. Geldhof, L. Vandevelde, and R. Boel, "A general description of high-frequency position estimators for interior permanent-magnet synchronous motors," in *International Conference on Electrical Machines (ICEM)*, Sept. 2004.

[14] J. Holtz, "Initial rotor polarity detection and sensorless control of pm synchronous machines," *IEEE Industry Applications Conference, 41st IAS Annual Meeting.*, vol. 4, pp. 2040 – 2047, Oct. 2006.

[15] O. Scaglione, M. Markovic, and Y. Perriard, "Exploitation of a new iron b-h phenomenon for the standstill position detection of pm motors," in *International Conference on Electrical Machines (ICEM)*, Sept. 2010.

[16] H. Mai, F. Dubas, D. Chamagne, and C. Espanet, "Optimal design of a surface mounted permanent magnet in-wheel motor for an urban hybrid vehicle," in *IEEE Vehicle Power and Propulsion Conference (VPPC)*, pp. 481 – 485, 2009.

[17] F. Gabriel, F. D. Belie, P. Druyts, X. Neyt, J. Melkebeek, and M. Acheroy, "Compensating the influence of the stator resistor and inverter nonlinearities in signal-injection based sensorless strategies," in *IEEE Vehicle Power and Propulsion Conference (VPPC'09)*, (Dearborn, USA), pp. 283 – 290, Sept. 2009.

[18] F. Gabriel, F. D. Belie, P. Druyts, and X. Neyt, "Strategy to detect and prevent the current zero-crossing for inverter powered drives," in *IEEE International Conference on Electrical Machines (ICEM'10)*, (Rome, Italy), Sept. 2010.

Fabien Gabriel received the Electromechanical Engineering degree from the Université Libre de Bruxelles in 2004. In 2005, he worked in the company IRM group, in the R&D department, on the design of electronic card for measurement systems. Between 2005 and 2007, he worked in project development and management for the building industry, in the company Axis-Engineering. Since then, he has been working as research engineer for the Royal Military Academy, Belgium, on power electric machines control techniques. He is currently working toward the Ph.D. degree.

Frederik De Belie (M'05) was born in Belgium in 1979. He received the Master degree in electromechanical engineering from Ghent University, Ghent, Belgium, in 2002, and the Ph.D. degree in March 2010. His present research interests include modelling theory and control-system theory applied to electrical drives and, in particular, sensorless control of synchronous machines.

Pascal Druyts received the M.Sc. degree in electrical engineering in 1991 and the postgraduate degree in automatic control in 1992, both from the Université Libre de Bruxelles, Brussels, Belgium. Since 1992, he is with the Signal and Image Centre of the Royal Military Academy in Brussels. His current research is on the modeling of EMI sensors and ground penetrating radars within the framework of mine clearance.

Xavier Neyt received the engineering degree (summa cum laude) from the Free University of Brussels (ULB) in 1994, a post-graduate degree in signal processing in 2004 and his PhD from the University of Liege in 2008. In 1995 he received the Frerichs Award from the ULB and the special IBM grant from the Belgian National Fund for Scientific Research (NFWO). Up to 2008, he has been working as research engineer for the Royal Military Academy, Belgium. In 1996-1997 he was visiting scientist at the French aerospace center (ONERA) and in 1999 at the German aerospace centre (DLR). In 1997-1999 he was responsible for the design of the image compression module of the European MSG satellite and in 2000-2005, responsible for the redesign of the ground processing of the scatterometer of the European ERS satellite following its gyroscope anomaly. Since 2009, he is associate professor at the Royal Military Academy of Belgium. His research interests include signal processing in general and applied to radar with emphasis on passive radars, array processing, space-time adaptive processing and aperture synthesis.

Philippe Lataire received a degree in electromechanical engineering in 1975 and a degree in doctor in applied sciences in 1982 from the Vrije Universiteit Brussel (VUB, Brussels, Belgium). He is presently full professor at the VUB in the field of power electronics, automatic control and electric drives. The prime factors of his research interest are in the field of electric drives, power electronics and control. The Department FirW – ETEC, headed by Prof. Philippe Lataire, developed research activities in the fields of sustainable mobility, computational electrochemistry, lighting, electric machines and power electronics applications.